

Multiple Folding States and Disorder of Ribosomal Protein SA, a Membrane Receptor for Laminin, Anticarcinogens, and Pathogens

Mohamed B. Ould-Abeih,^{†,‡,§} Isabelle Petit-Topin,^{†,‡} Nora Zidane,^{†,‡} Bruno Baron,^{||,⊥} and Hugues Bedouelle^{*,†,‡}

[†]Institut Pasteur, Unit of Molecular Prevention and Therapy of Human Diseases, Department of Infection and Epidemiology, rue du Dr. Roux, F-75015 Paris, France

[‡]CNRS, URA3012, rue du Dr. Roux, F-75015 Paris, France

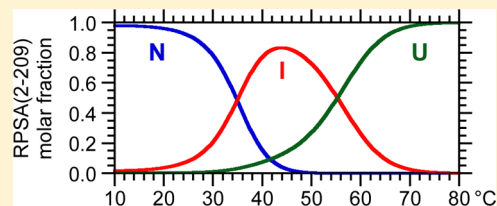
[§]Université Paris Diderot, Sorbonne Paris Cité, Cellule Pasteur, rue du Dr. Roux, F-75015 Paris, France

^{||}Institut Pasteur, Plate-forme de Biophysique des Macromolécules et de leurs Interactions, Department of Structural Biology and Chemistry, rue du Dr. Roux, F-75015 Paris, France

[⊥]CNRS, UMR3528, rue du Dr. Roux, 75015 Paris, France

Supporting Information

ABSTRACT: The human ribosomal protein SA (RPSA) is a multilocus protein, present in most cellular compartments. It is a multifunctional protein, which belongs to the ribosome but is also a membrane receptor for laminin, growth factors, prion, pathogenic microorganisms, toxins, and the anticarcinogen epigallocatechin gallate. It contributes to the crossing of the blood–brain barrier by neurotropic viruses and bacteria and is used as a biomarker of metastasis. RPSA includes an N-terminal domain, which is homologous to the prokaryotic ribosomal proteins S2, and a C-terminal extension, which is conserved in vertebrates. The structure of its N-domain has been determined from crystals grown at 17 °C. The structure of its C-domain remains unknown. We produced in *Escherichia coli* and purified the full-length RPSA and its N- and C-domains. We characterized the folding states of these recombinant proteins mainly by methods of fluorescence and circular dichroism spectrometry, in association with quantitative analyses of their unfolding equilibria, induced with heat or urea. The necessary equations were derived from first principles. The results showed that the N-domain unfolded according to a three-state equilibrium. The monomeric intermediate was predominant at the body temperature of 37 °C. It also existed in the full-length RPSA and bound ANS, a small fluorescent molecule. The C-domain was in an intrinsically disordered state. The recombinant N- and C-domains weakly interacted together. These results indicated a high plasticity of RPSA, which could be important for its multiple cellular localizations and functional interactions.



The human 40S ribosomal protein SA (RPSA) is a multilocus and multifunctional protein. It has many alternative names, including laminin receptor 1 (LamR1). The cDNA of the RPSA gene is formed by the assembly of seven exons, six of which correspond to the coding sequence. This cDNA does not include any signal sequence for addressing its protein product in the nucleus or cell membrane.^{1,2} The amino acid sequence of RPSA, deduced from the sequence of its cDNA, includes 295 residues and corresponds to a theoretical molecular mass (MM_{th}) of 32854 Da. RPSA can be subdivided into two main domains: an N-domain (residues 1–209), which corresponds to exons 2–5 of the gene, and a C-domain (residues 210–295), which corresponds to exons 6 and 7. Sequence analyses have shown that the N-domain of RPSA is homologous to ribosomal protein S2 (RPS2) of prokaryotes. It contains a palindromic ¹⁷³LMWWML¹⁷⁸ sequence that is conserved in all metazoans. Its C-domain is highly conserved in vertebrates. The amino acid sequence of RPSA is 98% identical in all mammals. These phylogenetic analyses have suggested that RPSA is a ribosomal protein that has acquired

the function of the laminin receptor during evolution.^{3,4} The crystal structure of a recombinant N-domain of RPSA (residues 1–220) has been determined at 2.15 Å resolution and found to be similar indeed to those of prokaryotic RPS2.⁵ The folding state and structure of its C-domain, which is highly negatively charged and includes five repeated motifs of sequence, remains unknown despite several molecular modeling attempts.^{6,7}

RPSA appears as polypeptides with apparent molecular masses (MM_{app}) of 37 and 67 kDa in immunoblots of cellular extracts. The 37 kDa form is a precursor of the 67 kDa form.^{8,9} RPSA is not glycosylated; it is acylated in position Ser2 by fatty acids, and this acylation is involved in its conversion to the 67 kDa form.^{10,11} Residue Tyr139 of RPSA is phosphorylated in vivo.¹²

RPSA is found associated with the cellular membrane,^{13–16} with the 40S subunit of ribosomes in the cytoplasm,^{17–20} with

Received: March 12, 2012

Revised: May 9, 2012

Published: May 28, 2012

DNA and some histones in the nucleus,^{20–22} and with the pre-ribosome in the nucleolus.²³

RPSA has numerous known functions. It interacts with the 18S rRNA and ribosomal protein S21 and plays a role in the maturation and assembly of the ribosome.^{7,17–20} RPSA is a component of the nuclear machinery.^{20–22} It is a membrane receptor for laminin and growth factors, e.g., Midkine.^{13,14,22,24,25} As such, it has a role in tumor invasion and aggressiveness.²⁶ RPSA is also a membrane receptor for toxins, prion, neurotropic viruses, and bacteria, of which it could promote adherence to the blood–brain barrier.^{16,27–32} RPSA is involved in signal transduction within the cell, e.g., through TIMAP (TGF- β -inhibited, membrane-associated protein) and PP-1 (protein phosphatase-1).³³ RPSA is a receptor for epigallocatechin gallate (EGCG), a major constituent of green tea, and mediates its anticarcinogenic activity via eEF1A (eukaryotic translation elongation factor 1A) and MYPT1 (myosin phosphatase targeting subunit 1).³⁴ Several of these functions have been specifically associated with the C-domain of RPSA.^{6,7,32,35,36}

A high proportion of eukaryotic proteins includes intrinsically disordered regions. These proteins are often multifunctional and interact with a large number of different partners.^{37–39} They are mainly involved in the following categories of functions: molecular assembly, molecular recognition and signaling, protein modification, and entropic chain activity.³⁷ RPSA fulfills at least three of these four categories of functions. Therefore, we asked the following questions. Given the multilocus and multifunction properties of RPSA, does this protein include disordered regions? Does the X-ray structure of its N-domain, which was determined from crystals grown at 17 °C, adequately represent its folding state in live mammals? What is the folding state of its C-domain, which is conserved in vertebrates and involved in several functions?

To approach these questions, we produced in *Escherichia coli* and purified the full-length RPSA, its ribosomal domain (N-domain), its vertebrate extension, and its acid domain (C-domains) in recombinant and homogeneous forms, in sufficient quantities for biophysical studies. We explored the folding states of these RPSA derivatives by methods of fluorescence and circular dichroism (CD) spectrometry, in association with quantitative analyses of their unfolding equilibria, induced by urea or heat. We also tested whether the N- and C-domains interact together by immunochemical methods.

Our results have shown that the C-domain of RPSA had little or no regular secondary structure, included local clusters of structure involving aromatic residues, reacted noncooperatively to the action of denaturing agents, and was not in a molten globular state. The N-domain unfolded according to a three-state equilibrium, including a monomeric intermediate. This intermediate was highly populated under some conditions, in particular at the body temperature of 37 °C. It also existed in the full-length RPSA and bound ANS, a small amphipathic fluorescent molecule. The N- and C-domains interacted weakly between them. These results have indicated a high plasticity of RPSA, which could be important for its localization in different cellular compartments and its numerous functions.

THEORY

Three-State Equilibrium of Unfolding. Let P be a monomeric protein, N its native folded state, I an intermediate state, and U its unfolded state. Let us assume that this protein unfolds according to the equilibria



Under physiological conditions, the protein is almost entirely in its native form (N) and the concentrations of states I and U cannot be detected. To be studied, the equilibria of unfolding are generally shifted with a denaturing agent, like urea or temperature. New equilibria form for each value x of denaturant. An unfolding profile is obtained by measuring a signal of the protein, sensitive to its conformational state, as a function of x . The equations derived in this and the following paragraphs allow one to determine the concentrations of N, I, and U for each value of x .

The laws of mass action and conservation give the following equations, where K_1 and K_2 are equilibrium constants and C (molar) is the total concentration of the protein:

$$[I]/[N] = K_1; [U]/[I] = K_2 \tag{2}$$

$$[N] + [I] + [U] = C \tag{3}$$

Generally, it is more convenient to reason with molar fractions:

$$f_n = [N]/C; f_i = [I]/C; f_u = [U]/C \tag{4}$$

Equation 3 can be rewritten as

$$f_n + f_i + f_u = 1 \tag{5}$$

From eqs 2 and 4, one deduces

$$f_i = K_1 f_n \text{ and } f_u = K_1 K_2 f_n \tag{6}$$

From eqs 5 and 6, one deduces

$$f_n = 1/(1 + K_1 + K_1 K_2) \tag{7}$$

Law of the Signal: Fluorescence Intensity. Let us assume that the intensity of fluorescence, for a set light of excitation, is used to monitor the unfolding equilibria of eq 1. If $Y_t(x)$ is the global signal of the unfolding mixture, the law of additivity of the signals applies to the fluorescence intensities:

$$Y_t(x) = [N]Y_n(x) + [I]Y_i(x) + [U]Y_u(x) + Y_d(x) \tag{8}$$

where Y_n , Y_i , and Y_u are the molar signals of state N, state I, and state U, respectively, and Y_d is the signal of the solvent. The signal of the solvent alone is generally measured in a separate experiment, and only the protein signal $Y(x)$ is considered:

$$Y = Y_t - Y_d(x) = [N]Y_n + [I]Y_i + [U]Y_u \tag{9}$$

$$Y = C(f_n Y_n + f_i Y_i + f_u Y_u) \tag{10}$$

Experimentally, one observes that $Y(x)$ is a linear function of x for the low and high values of denaturant,⁴⁰ and therefore, one writes for every x

$$Y_n(x) = y_n(1 + xh_n); \quad Y_i = n_i y_n = \text{constant}; \\ Y_u(x) = n_u y_n(1 + xh_u) \tag{11}$$

where h_n , n_i , n_u and h_u are intrinsic parameters of the protein. Y_i is taken to be a constant because the intermediate is usually present only in a narrow interval of x values. In some instances (see Results), the variation of $Y(x)$ for the low and high values of x may be better approximated by an exponential function. One therefore writes

$$Y_n(x) = y_n \exp[h_n(x_0 - x)]; \quad Y_i = n_i y_n = \text{constant}; \\ Y_u(x) = n_u y_n \exp[h_u(x_0 - x)] \tag{12}$$

Table 1. Plasmids for the Expression of RPSA and Its Derivatives in *E. coli*^a

plasmid	protein	exons	sequence
pAP1	RPSA(2–295)	2–7	mrgshhhhhhgSGAL-----TTEWS
pMOA5	RPSA(2–295)	2–7	mrgshhhhhhgSGAL-----TTEWSasawshpqfek
pMOA1	RPSA(2–209)	2–5	mrgshhhhhhgSGAL-----DPEEA
pMOA2	RPSA(2–220)	C2–6	mrgshhhhhhgSGAL-----AAEKa
pMOA3	RPSA(210–295)	6–7	mrgshhhhhhgSIEKE-----TTEWS
pMOA4	RPSA(225–295)	C6–7	mrgshhhhhhgSEEFQ-----TTEWS
pIT1	Flag-RPSA(225–295)	C6–7	mrgshhhhhhgSdykdddkgSSEEFQ-----TTEWS

^aIn column 2, the numbers in parentheses give the positions of the first and last residues of the RPSA fragment in the recombinant polypeptide. In column 3, C stands for included in; only the 3'-part of exon 2 and the 5'-part of exon 7 include coding sequences. In column 4, the N- and C-terminal residues of the RPSA fragment are uppercase whereas the residues of the tags are lowercase.

where x_0 is fixed and chosen in the transition region of the unfolding profile.

Analysis of the Unfolding Profiles. The combination of eqs 6, 7, 10, and 11 gives

$$Y = C_{y_n} [1 + xh_n + K_1n_i + K_1K_2n_u(1 + xh_u)] / (1 + K_1 + K_1K_2) \tag{13}$$

Likewise, the combination of eqs 6, 7, 10, and 12 gives

$$Y = C_{y_n} \{ \exp[h_n(x_0 - x)] + K_1n_i + K_1K_2n_u \exp[h_u(x_0 - x)] \} / (1 + K_1 + K_1K_2) \tag{14}$$

When the denaturant is a chemical molecule, e.g., urea, one generally assumes that the variation of free energy between two conformational states is a linear function of its concentration x , for example:^{41,42}

$$\Delta G = -RT \ln(K) = \Delta G(H_2O) - mx \tag{15}$$

and therefore

$$K_1 = \exp\{[m_1x - \Delta G_1(H_2O)]/RT\} \tag{16}$$

$$K_2 = \exp\{[m_2x - \Delta G_2(H_2O)]/RT\} \tag{17}$$

Equation 13, where K_1 and K_2 are developed as in eqs 16 and 17 and which relates the intensity of fluorescence to the concentration x of denaturant, was fit to the unfolding data with C_{y_n} , h_n , n_i , n_u , h_u , m_1 , m_2 , $\Delta G_1(H_2O)$, and $\Delta G_2(H_2O)$ as floating parameters.

When the denaturant is heat, the variation of free energy between two states is given by the Gibbs–Helmholtz equation.

$$\begin{aligned} \Delta G(T) &= -RT \ln(K) \\ &= \Delta H_m(1 - T/T_m) - \Delta C_p[(T_m - T) + T \ln(T/T_m)] \end{aligned} \tag{18}$$

where T_m is the temperature at which $\Delta G(T) = 0$, ΔH_m is the variation of enthalpy between the two considered states at T_m , and ΔC_p is the variation of caloric capacity between the two states. Therefore

$$K_1 = \exp(\{ \Delta C_{p1}[(T_{m1} - T) + T \ln(T/T_{m1})] - \Delta H_{m1}(1 - T/T_{m1}) \} / RT) \tag{19}$$

$$K_2 = \exp(\{ \Delta C_{p2}[(T_{m2} - T) + T \ln(T/T_{m2})] - \Delta H_{m2}(1 - T/T_{m2}) \} / RT) \tag{20}$$

An approximation $\Delta C_{p,th}$ of the global ΔC_p value between the N and U states can be calculated from the protein sequence.⁴² Therefore, $\Delta C_{p2} = \Delta C_{p,th} - \Delta C_{p1}$. Equation 13 or 14, where K_1 and K_2 are developed as in eqs 19 and 20 and which relates the intensity of fluorescence to the temperature $x = T$, was fit to the unfolding data with C_{y_n} , h_n , n_i , n_u , h_u , ΔH_{m1} , ΔH_{m2} , T_{m1} , T_{m2} , and ΔC_{p1} as floating parameters.

Two-State Equilibrium of Unfolding. In this well-documented case, one assumes that the protein unfolds according to the equilibrium $N \rightleftharpoons U$ with $[U]/[N] = K$ and $[N] + [U] = C$. The derivation of the equations is similar to that given above but simpler:⁴³

$$Y = C_{y_n} \{ n_u(1 + xh_u) + [1 + xh_n - n_u(1 + xh_u)] / (1 + K) \} \tag{21}$$

MATERIALS AND METHODS

Strains, Reagents, and Buffers. *E. coli* strain XL1-Blue (F':Tn10 *lacI^q/recA1, hsdR17*) was obtained from Stratagene and NEB Express I^q (miniF-*lacI^q/lon, ompT*) from New England Biolabs. Plasmid pQE30 was obtained from Qiagen and plasmid IRAKp961G21194Q2, which carries the *Mus musculus* RPSA gene, from RZPD (Deutsches Ressourcenzentrum für Genomforschung GmbH). All the plasmids carry the *bla* gene (Amp^R) except miniF-*lacI^q*, which carries the *cat* gene (Cam^R).

The culture media LB and 2-YT, NuPAGE Novex Bis-Tris 4 to 12% gradient gels, MES-SDS running buffer, sample buffer, and See Blue Plus 2 Prestained Standards were purchased from Invitrogen. IPTG was from Euromedex. PBS (phosphate-buffered saline), Tween 20, 4-nitrophenyl phosphate (pNPP), desthiobiotin, 1,8-ANS, and the conjugate between alkaline phosphatase and monoclonal antibody M2 to the Flag tag were from Sigma-Aldrich. Bovine serum albumin (BSA) was from Roche. Maxisorp ELISA plates were from Nunc. The fast-flow NiNTA and superflow Strep-Tactin resins were from Qiagen. Ultrapure urea was from MP Biochemicals. Ampicillin was used at 200 µg/mL, tetracycline at 15 µg/mL, and chloramphenicol at 25 µg/mL. The solutions of 10 M urea were prepared daily and their pH values adjusted as described previously.⁴¹ The concentrations of urea were measured with a refractometer and a precision of 0.01 M.

Buffer A contained 50 mM Tris-HCl, 500 mM NaCl, and imidazole (pH 8.2 at 4 °C). Buffer B contained 50 mM Tris-HCl, 300 mM NaCl, and 2.5 mM desthiobiotin (pH 8.0). Buffer C contained 10 mM potassium phosphate (pH 8.0). Buffer D contained 50 mM Tris-HCl and 150 mM NaCl (pH 8.2 at 20 °C). Buffer E contained 50 µg/mL ANS in buffer D.

Buffer F contained 100 $\mu\text{g}/\text{mL}$ ANS in buffer D. Buffer G contained 0.05% Tween 20 in PBS. Buffer H contained 3% BSA in buffer G. Buffer J contained 1% BSA in buffer G. Buffer K contained 0.1 M diethanolamine and 10 mM MgCl_2 (pH 9.8).

Genetic Constructions. The RPSA gene was amplified from plasmid IRAKp961G21194Q2 by polymerase chain reaction with two oligonucleotide primers that introduced a *Bam*HI restriction site at the 5'-end and a *Hind*III site at the 3'-end of the amplified DNA segment. The amplification product was inserted between the corresponding sites of plasmid pQE30. The recombinant plasmids were cloned by transformation into strain XL1-Blue and the recombinant strains grown at 30 °C. The expression plasmid thus obtained, pAP1, encoded residues 2–295 of the RPSA protein, under control of the promoter for the polymerase of phage T5 and *lacO* operator. To obtain 5'- or 3'-terminal segments of the RPSA gene encoding the N- or C-domains of RPSA, we introduced a second *Hind*III or *Bam*HI site into the gene by oligonucleotide site-directed mutagenesis of pAP1. The mutant derivatives of pAP1 were digested with the *Bam*HI or *Hind*III enzyme, circularized by ligation, and introduced into XL1-Blue as described above (Table 1). Plasmid pMOA5 was obtained by inserting a synthetic double-stranded DNA fragment 5'-gCCGGCGACC...GAAAAATGAtaagctt-3', encoding a hybrid polypeptide between residues 271–295 of RPSA and the Strep tag,⁴⁴ between the unique *Ngo*IV and *Hind*III sites of pAP1 (Table 1). Plasmid pIT1 was obtained by inserting a double-stranded DNA cassette, formed by hybridization of the two following oligonucleotides and encoding the Flag tag,⁴⁴ into the *Bam*HI site of plasmid pMOA4: 5'-GA TCT GAC TAC AAA GAC GAT GAC GAC AAA G-3' and 5'-GA TCC TTT GTC GTC ATC GTC TTT GTA GTC A-3'. All the genetic constructs were verified by DNA sequencing.

Production and Purification of the Recombinant Proteins. The RPSA derivatives were produced in the cytoplasm of strain NEB Express I⁹ from the plasmids listed in Table 1. A preculture of the producing strain was performed in LB medium, supplemented with ampicillin and chloramphenicol, overnight at 30 °C from a fresh and isolated colony. The preculture was diluted in 2-YT medium, supplemented with ampicillin, to obtain a starting absorbance A_{600} of 0.07–0.09. The culture was conducted at 30 °C until A_{600} reached 0.7–0.8, and then the expression of the recombinant gene was induced with 1.0 mM IPTG. The temperature and length of the induction phase were equal to 20 °C and overnight, respectively, for the bacteria harboring pMOA1 and pMOA2 and 30 °C and 4 h, respectively, for those harboring the other plasmids. The RPSA derivatives were purified at 4 °C through their hexahistidine tag via affinity chromatography on a column of NiNTA resin and elution with imidazole in buffer A. A second purification was performed for RPSA(2–295) through its Strep tag via affinity chromatography on a column of Strep-Tactin and elution with buffer B. The purification fractions were analyzed by sodium dodecyl sulfate–polyacrylamide gel electrophoresis (SDS–PAGE) under reducing conditions, and those that were pure (>95% homogeneous) were pooled, flash-frozen, and kept at –80 °C. The protein concentrations were measured by absorbance spectrometry. Aliquots of RPSA(210–295) and RPSA(225–295) were analyzed by mass spectrometry after extensive dialysis against 65 mM ammonium bicarbonate and lyophilization, as described previously.⁴⁵

Circular Dichroism Spectra. The proteins were dialyzed against buffer C prior to the circular dichroism (CD)

spectroscopy experiments. These experiments were performed with an Aviv model 215 CD spectrometer equipped with a thermoelectric cuvette holder. The CD spectra were recorded at 20 °C between 190 and 260 nm with a quartz cell with a path length of 0.02 cm in the far-UV region and between 250 and 350 nm with a quartz cell with a path length of 1 cm in the near-UV region. The signal was acquired for 1 s at each wavelength; the wavelength increment was equal to 1 nm and the scan rate to 1 nm/s. Each spectrum represents the average of three scans. The signal for the solvent alone was subtracted from the raw signal. The measurements are reported as molar circular dichroism per residue $\Delta\epsilon$ (millidegrees per molar per centimeter).

Fluorescence Measurements. The fluorescence spectra were recorded with a FP-6300 spectrofluorometer (Jasco) in a quartz cuvette (10 mm \times 2 mm) at 20 °C. The spectra of intrinsic fluorescence were recorded between 310 and 370 nm with excitation at 278 nm in buffer D. The spectra of ANS fluorescence were recorded between 440 and 540 nm with excitation at 372 nm in buffer E. The slit width was equal to 2.5 nm for the excitation light and 5 nm for the emission. The wavelength increment was equal to 0.5 nm. The fluorescence signal for the protein was obtained by subtraction of the signal for the solvent alone.

Unfolding with Urea. Unfolding with urea was performed as described previously.⁴¹ Each reaction mixture (1 mL) contained purified protein (10 $\mu\text{g}/\text{mL}$) and varying concentrations of urea (0–8 M) in buffer D or E. Control reaction mixtures were prepared by replacing the protein with buffer. The mixtures were incubated for 16 h at 20 °C to permit the unfolding reactions to reach equilibrium. To test the reversibility of the unfolding reaction, a protein sample was denatured in 8 M urea and buffer D for 4 h. The denatured protein was diluted with buffer D to reach a final urea concentration between 8 and 1 M. The diluted mixture was then incubated for 16 h at 20 °C to allow the reaction to reach equilibrium as described above. The concentration of urea was measured in each reaction mixture after completion of the experiments. The equilibria of unfolding were monitored with the intrinsic fluorescence of proteins or the extrinsic fluorescence of ANS as described in the previous paragraph.

Thermal Unfolding. Heat-induced denaturations were performed either with a Quantamaster spectrofluorometer (Photon Technology International) or with an Aviv model 215 CD spectrometer, both equipped with a computer-operated thermoelectric cuvette holder. In both cases, the signal for the protein was obtained by subtraction of the signal for the solvent alone, recorded in a separate experiment. In the first case, the purified proteins (20 $\mu\text{g}/\text{mL}$ in buffer D or F) were melted in a quartz cuvette (10 mm \times 10 mm) with a constant heating rate of 0.25 °C/min between 4 and 85 °C. The intrinsic fluorescence was excited at 278 nm, and the emission was recorded at 330 and 350 nm. The ANS fluorescence was excited at 372 nm, and the emission was recorded at 475 and 530 nm. The excitation and emission slit widths were equal to 1 and 10 nm, respectively.

In the second case, the purified proteins (100 $\mu\text{g}/\text{mL}$ in buffer C) were melted in a quartz cuvette (path lengths of 2 mm) with a constant heating rate of 0.2 °C/min between 10 and 95 °C in 1 °C steps. The time to heat the reaction and the time to acquire the far-UV CD spectrum were equal to 5 min each at each step of temperature. A renaturation step of the

proteins was performed at 25 °C for 30 min after each full cycle of denaturation.

Indirect Enzyme-Linked Immunosorbent Assays (ELISAs). ELISAs were performed in 96-well microtiter plates with a volume of 100 μ L/well. For the sensitization of the plates, a solution of RPSA(2–209) (2 μ g/mL) in PBS or PBS alone as a control was loaded in the wells and the plate was incubated overnight at 4 °C so adsorption could occur. The wells were washed with buffer G (five times), blocked with buffer H, and then washed as described above. For the capture of the C-domain by the immobilized N-domains, the purified preparation of Flag-RPSA(225–295) was diluted in buffer J, the wells were loaded with the diluted protein or buffer J alone as a blank sample, and the plate was incubated for 1 h at 25 °C. The wells were washed as described above, and the bound Flag-RPSA(225–295) was detected with a conjugate between alkaline phosphatase and an antibody to the Flag tag. More precisely, a 3300-fold dilution of the conjugate in buffer J was added to the wells, and the plate was incubated for 1 h at room temperature for the capture of the conjugate. The wells were washed as described above, and the bound conjugate was detected by addition of 5 mM pNPP in buffer K and measurement of A_{405} .

Analysis of the Sequence, Structure, and Experimental Data. The sequences of the *Homo sapiens* and *M. musculus* RPSA genes and their transcripts, exons, and encoded proteins were retrieved with the Ensembl genome browser (<http://www.ensembl.org>). The sequences of the RPSA proteins from *H. sapiens* (UniProt entry P08865) and *M. musculus* (UniProt entry P14206) were also retrieved from the UniProtKB database (<http://www.uniprot.org>). They differ by only one amino acid residue, Asp293 in humans and Glu293 in mice. We used the murine cDNA and protein in our study for regulatory reasons. The sequences of RPSA and ribosomal proteins S2 from *E. coli* (UniProt entry P0ATV0), *Thermus thermophilus* (UniProt entry P80371), and *Aeroglobus fulgidus* (UniProt entry O29132) were aligned with ClustalW.⁴⁶ The disordered regions of RPSA were predicted with MeDor, a metaserver for predicting protein disorder.⁴⁷ MM_{th} , pI, and molar extinction coefficient values were computed from the amino acid sequences with subprogram PepStat of the EMBOSS software suite.⁴⁸

We used the CDSSTR method and reference Set 7, as implemented in DICHROWEB, to deconvolute the CD spectra and estimate the secondary structure contents of the proteins.^{49,50} The atomic coordinates of the RPSA ribosomal domain [Protein Data Bank (PDB) entry 3BCH], *E. coli* ribosome (PDB entry 2AVY), and *T. thermophilus* ribosome (PDB entry 1JSE) were retrieved from the PDB (<http://www.rcsb.org>). The solvent accessible surface areas (ASA) were computed with the access routine of What If and a probe radius of 1.4 Å.⁵¹ The structures were drawn with RasMol version 2.7.3 (<http://www.rasmol.org>).

We performed the curve fits with either Kaleidagraph (Synergy Software) or pro Fit version 6.0.6 (Quantum Soft) for the more demanding cases and used a Levenberg–Marquardt algorithm in both cases. Kaleidagraph gives Pearson's coefficient of correlation, R_p . The values of the molar fractions, f_n , f_v , and f_w and of their roots were calculated with pro Fit. The standard error (SE) on a sum of two terms A and B was calculated from the equation of error propagation: $SE(A + B)^2 = SE(A)^2 + SE(B)^2$.

RESULTS

Production and Purification of RPSA and Its Domains.

We constructed recombinant plasmids for the expression of RPSA and its main domains in *E. coli*, and their purification to homogeneity (Table 1). For their design, we used the observation that the sites of introns in eukaryotic genes often correspond to the limits of functional domains or modules in the encoded proteins.^{52,53} RPSA(2–295) corresponded to the full-length protein, RPSA(2–209) exactly to exons 2–5 of the RPSA gene, RPSA(2–220) to the protein domain that has been crystallized,⁵ RPSA(210–295) exactly to exons 6 and 7, and RPSA(225–295) to the C-terminal acid domain of the protein. RPSA(2–209) also corresponded to the ribosomal domain of RPSA and included all the residues that are visible in the crystal structure of RPSA(2–220), i.e., residues 9–205. RPSA(210–295) also corresponded to the domain of RPSA that is conserved in vertebrates.³ RPSA(225–295) included all five repetitions of the E/D-W-S/T motif, 13 negative charges, and no positive charge.

All the constructions included an N-terminal hexahistidine His tag. RPSA(2–295) included a C-terminal Strep tag in addition. We constructed two versions of RPSA(225–295), one with an N-terminal His tag and the other, named Flag-RPSA(225–295), with two N-terminal tags, a His tag and a Flag tag (Materials and Methods).⁴⁴

An analysis by SDS–PAGE under reducing conditions showed that the RPSA derivatives described above could be purified to homogeneity through their His tag, except RPSA(2–295). We observed discrete polypeptide species that had mobilities intermediate between those of RPSA(2–295) and RPSA(2–209) and suggested a partial proteolysis of RPSA(2–295) within its C-domain. RPSA(2–295) was purified to homogeneity in two steps, first through its N-terminal His tag and then through its C-terminal Strep tag (Figure S1 of the Supporting Information). We deduced the following values of the ratio MM_{app}/MM_{th} between the apparent and theoretical molecular masses from these SDS–PAGE analyses (Figure S1 of the Supporting Information): 1.17 for RPSA(2–295), 0.85 for RPSA(2–209), 0.92 for RPSA(2–220), 2.28 for RPSA(210–295), and 2.17 for RPSA(225–295). These values were consistent with a weak binding of SDS to the acid domain of RPSA and explained the difference between the values for RPSA ($MM_{app} = 37000$ Da, and $MM_{th} = 32854$ Da) that have been reported previously.^{9,54}

The experimental molecular masses of the recombinant C-domains, measured by mass spectrometry, corresponded exactly to their MM_{th} values: 10789.47 and 10789.56 Da for RPSA(210–295) and 9162.66 and 9162.74 Da for RPSA(225–295), respectively. RPSA(210–295) and RPSA(225–295) have predicted pI values of 4.24 and 4.15, respectively. Therefore, they are negatively charged, and their molecules should repulse each other at pH 8.2. Consistent with this prediction, we found that RPSA(210–295) at a concentration of 0.27 mM (2.9 mg/mL) gave a protein peak that was unique, sharp, and symmetrical when submitted to size exclusion chromatography in buffer D (Figure S2 of the Supporting Information). Previous studies have shown that RPSA(2–220) and a recombinant full-length RPSA are monomeric in solution.^{5,55} We confirmed that full-length RPSA(2–295) and its isolated N-domains, RPSA(2–209) and RPSA(2–220), bound laminin in an indirect ELISA, as previously reported (data not shown).^{5,25}

Structure of RPSA As Analyzed by CD. We recorded the CD spectra of the RPSA derivatives in the far-UV region at 20 °C to gain information about their contents in secondary structures (Figure 1). Spectra of α -helices generally include two

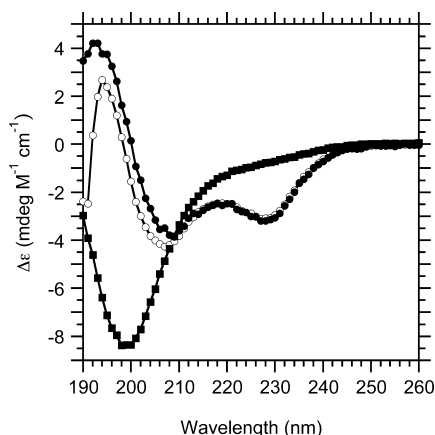


Figure 1. Far-UV CD spectra of RPSA derivatives. $\Delta\epsilon$ is the molar circular dichroism per residue: (●) RPSA(2–209), (○) RPSA(2–295), and (■) RPSA(210–295).

characteristic local minima at wavelengths of 208 and 222 nm. The latter minimum was shifted from 222 to 228 nm for RPSA and its N-domains. This shift could be due to a contribution of their aromatic residues.⁵⁶ Deconvolutions showed that the spectra of RPSA and its N-domains were characteristic of proteins that include both α -helices and β -sheets. The secondary structure content of RPSA(2–209), deduced from its spectra, was consistent with the crystal structure of the N-domain.⁵ In contrast, the spectra of RPSA(210–295) and RPSA(225–295) were characteristic of proteins that include a majority of random coil residues (Table 2).

We also recorded the spectra of RPSA(210–295) and RPSA(225–295) in the near-UV region (Figure 2 and Figure S3 of the Supporting Information). The spectra show two peaks at 262 and 268 nm, characteristic of Phe residues, and a positive signal between 280 and 295 nm, which we attributed to Trp residues because the C-domains did not include any Tyr residue. These results showed the existence of interactions between the aromatic residues Phe and Trp of the C-domains and their electronic and structural environments.⁵⁷

Unfolding with Urea and Monitoring via Intrinsic Fluorescence. We characterized the unfolding equilibria of the RPSA derivatives, induced with urea, to explore their folding states. These equilibria were monitored through the intrinsic fluorescence of the proteins upon excitation at 278 nm. RPSA(2–209) and RPSA(2–220) included four Trp residues

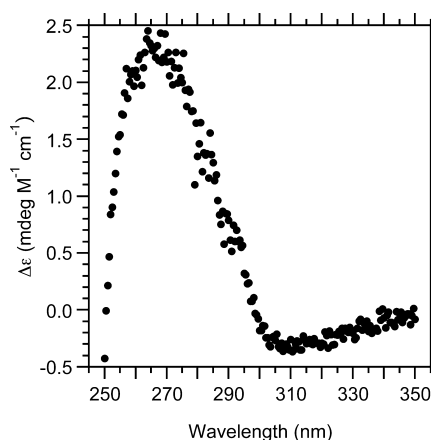


Figure 2. Near-UV CD spectrum of RPSA(210–295). $\Delta\epsilon$ is the molar circular dichroism.

and seven Tyr residues. RPSA(210–295) and RPSA(225–295) included six Trp residues. The Strep tag, which was present in RPSA(2–295), included one additional Trp residue. The four Trp residues of the N-domain are buried in the core of the protein, according to the crystal structure.⁵ We recorded the fluorescence spectra of the RPSA derivatives in 0 and 8 M urea at 20 °C (Figures S4–S7 of the Supporting Information). For RPSA(2–209) and RPSA(2–220), wavelength λ_{\max} of the maximal intensity of fluorescence was equal to 330 nm in the absence of urea and consistent with Trp residues in a hydrophobic environment. For RPSA(210–295) and RPSA(225–295), the value of λ_{\max} was equal to 351 nm and consistent with Trp residues in a polar environment. For RPSA(2–295), λ_{\max} had an intermediate value, 340 nm. The value of λ_{\max} was equal to 350 nm in the presence of 8 M urea for all the RPSA derivatives. The fluorescence intensities of full-length RPSA and its N-domains were lower in 8 M urea than in 0 M urea below 357 nm, whereas those of the C-domains were higher.

The unfolding profiles of the N-domains, RPSA(2–209) and RPSA(2–220), showed two cooperative transitions (Figure 3 and Figure S8 of the Supporting Information). We checked that the refolding profile of RPSA(2–209), reached from its unfolded state in 8 M urea, was similar to its unfolding profile (data not shown). We modeled the unfolding equilibria with a three-state system, composed of native state N, intermediate state I, and unfolded state U (eqs 13, 16, and 17 in Theory). The fitting of this model to the experimental data allowed us to determine four characteristic thermodynamic parameters: the differences in free energy between N and I in the absence of urea [$\Delta G_1(\text{H}_2\text{O})$] and between I and U [$\Delta G_2(\text{H}_2\text{O})$] and their coefficients of dependence toward the concentration of urea

Table 2. Secondary Structure Contents of RPSA Derivatives, As Deduced from Their Far-UV CD Spectra^a

	helix 1	helix 2	strand 1	strand 2	turns	unordered	total
RPSA(2–295)	0.34	0.19	0.10	0.07	0.14	0.16	1.00
RPSA(2–220)	0.21	0.16	0.09	0.07	0.19	0.28	1.00
RPSA(2–209)	0.29	0.19	0.09	0.05	0.15	0.23	1.00
RPSA(210–295)	0.01	0.04	0.06	0.03	0.07	0.80	1.01
weighted sum	0.20	0.14	0.08	0.04	0.13	0.41	1.00
RPSA(225–295)	0.01	0.04	0.06	0.03	0.06	0.81	1.01

^aRow 5 lists the secondary structure contents for the union of the isolated RPSA(2–209) and RPSA(210–295) domains, calculated as the sum of their individual contents, weighted by the number of residues (220 and 98, respectively).

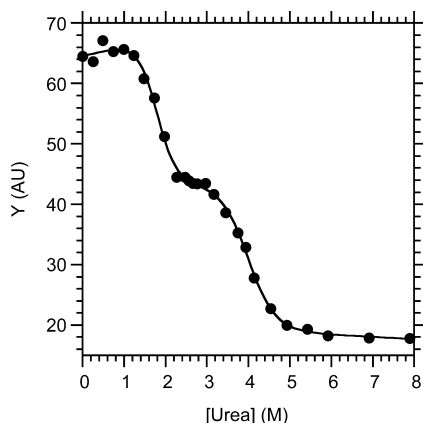


Figure 3. Unfolding equilibria of RPSA(2–209), induced with urea at 20 °C in buffer D and monitored through its intrinsic fluorescence. The protein was excited at 278 nm and its fluorescence intensity *Y* recorded at 330 nm in arbitrary units (AU). The solid line corresponds to the fitting of eqs 13, 16, and 17 to the experimental data ($R_p = 0.9968$).

(m_1 and m_2 , respectively), which characterize the cooperativity of the unfolding transitions.⁴² It also allowed us to determine the relative fluorescences n_i and n_u of states I and U, respectively, in the absence of urea. We then calculated the molar fractions f_N , f_I , and f_U of the three states as a function of urea concentration, using eqs 6 and 7 (Table 3 and Figure 4).

Table 3. Characteristic Parameters of Unfolding Equilibria, Induced with Urea at 20 °C and Monitored through the Intrinsic Fluorescence Intensity^a

	RPSA(2–209)	RPSA(2–220)	RPSA(2–295)
m_1 (kcal mol ⁻¹ M ⁻¹)	2.49 ± 0.75	1.71 ± 0.47	0.79 ± 0.04
$\Delta G_1(\text{H}_2\text{O})$ (kcal mol ⁻¹)	4.44 ± 1.42	3.54 ± 0.96	2.13 ± 0.19
m_2 (kcal mol ⁻¹ M ⁻¹)	1.78 ± 0.51	1.61 ± 0.47	na ^b
$\Delta G_2(\text{H}_2\text{O})$ (kcal mol ⁻¹)	7.11 ± 1.99	6.30 ± 1.97	na ^b
$n_i = Y_i/Y_n(0)$	0.67 ± 0.02	0.70 ± 0.07	na ^b
$n_u = Y_u(0)/Y_n(0)$	0.32 ± 0.09	0.31 ± 0.07	0.42 ± 0.01
m (kcal mol ⁻¹ M ⁻¹)	4.28 ± 0.90	3.33 ± 0.67	0.79 ± 0.04
$\Delta G(\text{H}_2\text{O})$ (kcal mol ⁻¹)	11.55 ± 2.44	9.84 ± 2.19	2.13 ± 0.19
$\text{max}f_i$	0.96	0.87	na ^b
$f_N^{-1}(0.5)$ (M)	1.78	2.06	2.69
$f_I^{-1}(\text{max}f_i)$ (M)	2.74	2.97	na ^b
$f_U^{-1}(0.5)$ (M)	3.98	3.91	2.69

^aThe fluorescence intensity *Y* was measured at 330 nm for RPSA(2–209), 327 nm for RPSA(2–220), and 325 nm for RPSA(2–295). The values of the parameters and associated standard errors in rows 1–6 were obtained by fitting the equations of the equilibrium to the fluorescence data as described in Theory. The values of $\Delta G(\text{H}_2\text{O}) = \Delta G_1(\text{H}_2\text{O}) + \Delta G_2(\text{H}_2\text{O})$, $m = m_1 + m_2$, and their associated errors were calculated from the values for the constituent parameters. n_i and n_u are the relative fluorescence intensities of states I and U, respectively, in 0 M urea; f_N , f_I , and f_U are the molar fractions of states N, I, and U, respectively. ^bNot applicable.

The unfolding profile of the C-domain, RPSA(210–295), was noncooperative (Figure S9 of the Supporting Information). Its fluorescence intensity $Y(x)$, measured at a λ_{em} of 351 nm, increased with the concentration x of urea according to the linear law $Y(x)/Y(0) = 1 + hx$, where $h = 0.077 \pm 0.002 \text{ M}^{-1}$ (mean ± SE in the curve fit) and $R_p = 0.9975$ (Pearson

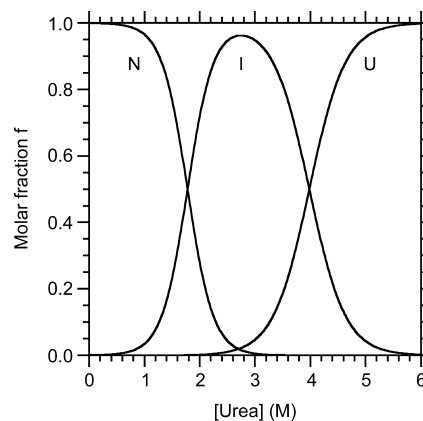


Figure 4. Molar fractions f_N , f_I , and f_U of native N, intermediate I, and unfolded U states of RPSA(2–209) at 20 °C in buffer D as a function of urea concentration. These fractions were calculated from the values of m_1 , $\Delta G_1(\text{H}_2\text{O})$, m_2 , and $\Delta G_2(\text{H}_2\text{O})$ in Table 3 through eqs 6 and 7.

correlation coefficient). Such a linear variation has already been reported for the Trp amino acid with a similar value for h of $0.050 \pm 0.001 \text{ M}^{-1}$ even though the experimental conditions were slightly different ($\lambda_{ex} = 290 \text{ nm}$, and $\lambda_{em} = 354 \text{ nm}$).⁴³ Therefore, the six Trp residues of RPSA(210–295) emitted fluorescence much like the free Trp amino acid in solution.

The unfolding profile of RPSA(2–295) showed a single cooperative transition (Figure S10 of the Supporting Information). We modeled its unfolding equilibria with a two-state system, native state N and unfolded state U (eq 21). The values of m and $\Delta G(\text{H}_2\text{O})$ thus obtained for RPSA(2–295) were much lower than those for the N-domains (Table 3). Moreover, the m value was much lower than the expected value for a protein of its length.⁴² These results indicated that RPSA(2–295) unfolded according to a mechanism with more than two states despite the observation of a single transition.

Unfolding with Heat and Monitoring through Intrinsic Fluorescence. We observed intermediate state I in the unfolding with urea (previous paragraph). To test whether such an intermediate existed under physiological conditions, we induced the unfolding equilibria of the RPSA derivatives with heat. These equilibria were monitored through the intrinsic fluorescence intensity upon excitation at 278 nm, as described above. We used a slow linear gradient of temperature, 0.25 K min^{-1} between 277 and 358 K (4 and 85 °C, respectively), so that the experiments were performed under quasi-equilibrium conditions.

The unfolding profiles of RPSA(2–209) and RPSA(2–220), induced with heat, showed two cooperative transitions (Figure 5 and Figure S11 of the Supporting Information). We modeled the unfolding equilibria again with a three-state system, N, I, and U (eqs 13, 19, and 20). The model depended on six thermodynamic parameters: temperatures T_{m1} and T_{m2} at which the variations of free energy $\Delta G_1(T)$ between states N and I and $\Delta G_2(T)$ between states I and U, respectively, were nil; the variations of enthalpy ΔH_{m1} between states N and I at temperature T_{m1} and ΔH_{m2} between states I and U at temperature T_{m2} ; and the variations of heat capacity ΔC_{p1} between states N and I and ΔC_{p2} between states I and U. We reduced this number to five characteristic parameters by empirically predicting the total heat capacity of the proteins ($\Delta C_{p,th} = \Delta C_{p1} + \Delta C_{p2}$), as described previously (Table 4).⁴² We then calculated the molar fractions f_N , f_I , and f_U of the three

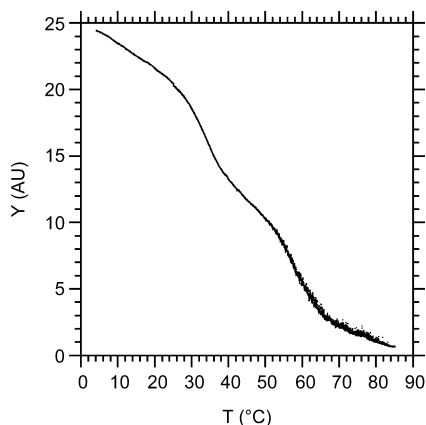


Figure 5. Unfolding equilibria of RPSA(2–209), induced with heat in buffer D and monitored through its intrinsic fluorescence. The protein was excited at 278 nm and its fluorescence intensity Y recorded at 330 nm. Equations 13, 19, and 20 were fit to the 5361 experimental data points with a $\Delta C_{p,th}$ of $3.70 \text{ kcal mol}^{-1} \text{ K}^{-1}$. The fitted curve and fluorescence trace are fully superposed within the experimental temperature range.

states as a function of temperature with eqs 6 and 7 (Table 5 and Figure S12 of the Supporting Information).

Table 4. Thermodynamic Parameters of Unfolding Equilibria, Induced with Heat and Monitored through the Intrinsic Fluorescence Intensity^a

	RPSA(2–209)	RPSA(2–220)	RPSA(2–295)
T_{m1} (K)	308.08 ± 0.07	307.94 ± 0.04	312.27 ± 0.01
ΔH_{m1} (kcal mol ⁻¹)	55.07 ± 0.71	59.47 ± 0.24	114.62 ± 0.14
T_{m2} (K)	328.42 ± 0.07	331.28 ± 0.19	na ^b
ΔH_{m2} (kcal mol ⁻¹)	43.82 ± 0.46	32.81 ± 0.47	na ^b
ΔC_{p1} (kcal mol ⁻¹ K ⁻¹)	2.09 ± 0.06	2.92 ± 0.06	na ^b
$\Delta C_{p,th}$ (kcal mol ⁻¹ K ⁻¹)	3.70	3.90	5.40
$\max f_i$	0.83	0.83	na ^b
$f_i^{-1}(\max f_i)$ (K)	317.03	316.79	na ^b

^aThe fluorescence intensity Y was measured at 330 nm. The values of the parameters and associated standard errors in rows 1–5 were obtained by fitting the equations of equilibrium to the fluorescence data as described in Theory. f_i is the molar fraction of state I. ^bNot applicable.

Table 5. Characteristic Parameters of Unfolding Equilibria, Monitored through the Intrinsic Fluorescence Intensity, at Several Temperatures^a

	T (°C)	RPSA(2–209)	RPSA(2–220)	RPSA(2–295)
f_n	17	0.97	0.96	1.00
f_n	20	0.96	0.95	1.00
Y_i/Y_n	20	0.59	0.58	na ^b
Y_u/Y_n	20	0.29	0.10	0.35
f_n	25	0.91	0.91	1.00
f_n	37	0.33	0.30	0.77
f_i	37	0.62	0.63	na ^b
f_u	37	0.05	0.06	0.23

^a f_n , f_i , and f_u are the molar fractions of states N, I, and U, respectively. Y_n , Y_i , and Y_u are the molar intensities of fluorescence. These parameters complement those listed in Table 4; see Theory for their calculations. ^bNot applicable.

The unfolding profile of RPSA(210–295) was noncooperative (Figure S13 of the Supporting Information). Its fluorescence intensity $Y(T)$, measured at a λ_{em} of 330 nm, decreased with temperature according to the exponential law $Y(T)/Y(310.15) = \exp[h(310.15 - T)]$, where $h = (2642.6 \pm 2.5) \times 10^{-5}$ ($R_p = 0.9982$). As a control, we monitored the fluorescence intensity $Y(T)$ of *N*-acetyl-L-tryptophanamide, a close analogue of a Trp residue (Figure S13 of the Supporting Information). It decreased with temperature according to the same exponential law, where $h = (2174.1 \pm 4.5) \times 10^{-5}$ ($R_p = 0.9899$). This comparison confirmed that the six Trp residues of RPSA(210–295) emitted fluorescence much like a free Trp residue in solution.

We also monitored the thermal unfolding of RPSA(210–295) through its far-UV CD at 207 nm (Figure S14 of the Supporting Information). We observed a noncooperative reversible transition that could be modeled by a linear function:

$$\Delta\epsilon(T)/\Delta\epsilon(310.15) = 1 + [(234.2 \pm 2.8) \times 10^{-5}] (310.15 - T); \quad R_p = 0.9935$$

where $\Delta\epsilon$ (millidegrees per molar per centimeter) is the molar circular dichroism per residue.

The unfolding profile of RPSA(2–295) showed a single cooperative transition that we modeled with a two-state system (Tables 4 and 5). We noticed a small deviation between the 6496 experimental data points and the fitted curve above 42 °C (Figure S15 of the Supporting Information). We therefore analyzed these data points with a phase diagram.⁵⁸ For a two-state system, the laws of signal and mass conservation imply that the fluorescence intensities at two different wavelengths, e.g., Y_{330} at 330 nm and Y_{350} at 350 nm, should be related by a linear function whose coefficients are independent of the molar fractions and therefore denaturant value. If one plots Y_{350} as a function of Y_{330} , a deviation from linearity in the resulting phase diagram indicates that the system involves more than two states. We observed that the 2243 couples (Y_{330} , Y_{350}) of data points below 32 °C were linearly related, as well as the 3451 couples of data points above 42 °C. The difference between the slopes of the two straight lines, 0.1663 ± 0.0008 , was significantly different from zero. The 802 couples of data points between 32 and 42 °C drew a smooth curve joining the two different straight lines (Figure 6). This very sensitive analysis showed the existence of three-state equilibria between 32 and 42 °C, and in particular at 37 °C, for RPSA(2–295). We also analyzed the unfolding profile of RPSA(2–209) with a similar phase diagram and thus confirmed the existence of three-state equilibria (Figure S16 of the Supporting Information).

Unfolding with Urea and Monitoring through ANS Fluorescence. We observed that the N-domain of RPSA unfolded according to a three-state system, including an intermediate state I, in urea, monitored through the intrinsic fluorescence intensity. However, these experimental conditions did not allow us to observe an intermediate for full-length RPSA. To gain information about this intermediate and attempt to detect it for full-length RPSA, we monitored the unfolding equilibria of RPSA(2–209), RPSA(2–220), and RPSA(2–295), induced with urea, through the extrinsic fluorescence of ANS or, more precisely, through its variation of intensity between experiments performed in the presence and absence of protein (Figure 7 and Figure S17 of the Supporting Information). The ANS quantum yield of fluorescence

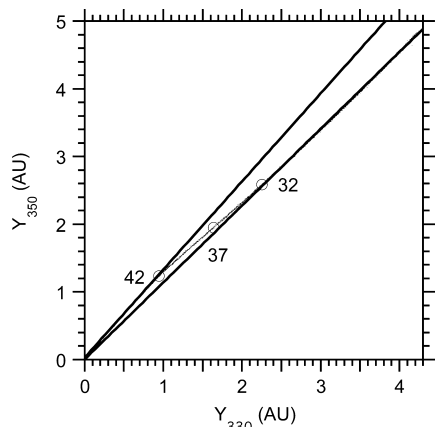


Figure 6. Phase diagram for the unfolding of RPSA(2–295), induced with heat in buffer D and monitored through its intrinsic fluorescence. The protein was excited at 278 nm, and its fluorescence intensities, Y_{330} and Y_{350} , were recorded at 330 and 350 nm, respectively, in arbitrary units (AU). The theory predicts that the phase diagram is linear for a two-state system. The empty circles correspond to temperatures of 32, 37, and 42 °C. The diagram was drawn from 6496 experimental data points. These data points were recorded in the same experiment as those of Figure S15 of the Supporting Information. The top straight line was obtained by fitting to the 3451 data points above 42 °C and the bottom straight line by fitting to the 2243 data points below 32 °C. The slopes of the straight lines were equal to 1.1357 ± 0.0005 ($R_p = 0.9997$) and 1.3020 ± 0.0006 ($R_p = 0.9996$), respectively, where the numbers correspond to the value of the slope and its standard error in the curve fit. The difference between the two slopes, 0.1663 ± 0.0008 , was highly significant. The curved part of the diagram corresponds to a range of temperatures over which three states, N, I, and U, were simultaneously in equilibrium.

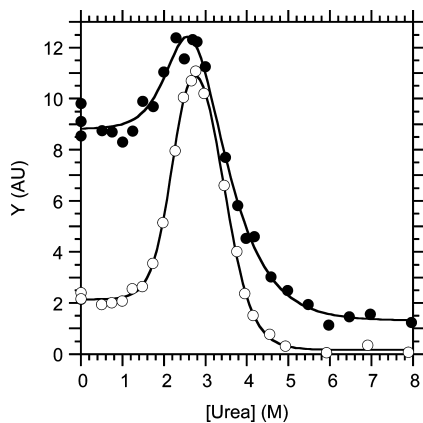


Figure 7. Unfolding equilibria of RPSA(2–220) and RPSA(2–295), induced with urea at 20 °C in buffer E and monitored through the fluorescence intensity Y of ANS. The figure was drawn for identical molar concentrations of the two proteins: (●) RPSA(2–295) and (○) RPSA(2–220). The solid lines correspond to the fitting of eqs 13, 16, and 17 to the experimental data with $h_n = h_u = 0$ fixed ($R_p = 0.9992$ and 0.9950, respectively).

emission is low in an aqueous environment and much higher in a hydrophobic environment.⁵⁹ We observed two cooperative transitions of unfolding for the three proteins described above, first between native state N, corresponding to a low fluorescence intensity of ANS, and intermediate I, characterized by a high fluorescence intensity, and then between I and unfolded state U, corresponding to a very low or nil fluorescence intensity. We analyzed these profiles with the

same model and the same equations that were used above, when the equilibria were monitored through the intrinsic fluorescence of proteins (eqs 13, 16, and 17; Table 6). We thus showed the existence of an intermediate of unfolding for full-length RPSA.

Table 6. Characteristic Parameters of Unfolding Equilibria, Induced with Urea at 20 °C and Monitored through the Fluorescence Intensity of ANS^a

	RPSA(2–209)	RPSA(2–220)	RPSA(2–295)
m_1 (kcal mol ⁻¹ M ⁻¹)	0.81 ± 0.30	2.31 ± 0.16	1.56 ± 0.52
$\Delta G_1(\text{H}_2\text{O})$ (kcal mol ⁻¹)	1.97 ± 0.40	5.14 ± 0.31	4.14 ± 0.77
m_2 (kcal mol ⁻¹ M ⁻¹)	1.34 ± 0.13	1.72 ± 0.12	0.82 ± 0.26
$\Delta_2 G(\text{H}_2\text{O})$ (kcal mol ⁻¹)	4.40 ± 0.79	5.88 ± 0.48	2.26 ± 1.66
$\text{max}f_i$	0.51	0.79	0.37
$f_n^{-1}(0.5)$ (M)	2.36	2.22	2.46
$f_i^{-1}(\text{max}f_i)$ (M)	2.82	2.78	2.84
$f_u^{-1}(0.5)$ (M)	3.38	3.43	2.99

^aThe values of the parameters and associated standard errors in rows 1–4 were obtained by fitting the equations of equilibrium to the fluorescence data as described in Theory. f_n , f_i , and f_u are the molar fractions of states N, I, and U, respectively.

We found that the fluorescence spectra of ANS were not significantly different in the presence and absence of RPSA(210–295), with a variation of <2% (data not shown).

Unfolding with Heat and Monitoring through ANS Fluorescence. Similarly, we followed the unfolding equilibria, induced with heat, through the extrinsic fluorescence of ANS for RPSA(2–209), RPSA(2–220), and RPSA(2–295). We observed two cooperative transitions for these three proteins (Figure 8 and Figures S18 and S19 of the Supporting

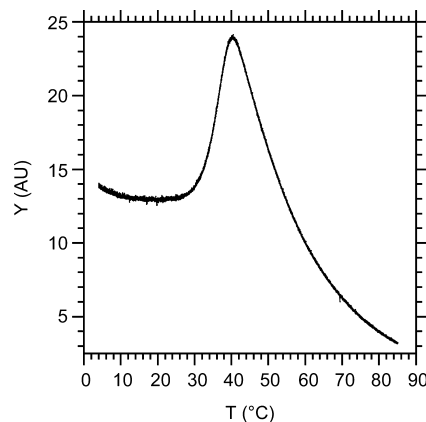


Figure 8. Unfolding equilibria of RPSA(2–295), induced with heat in buffer F and monitored through the fluorescence intensity Y of ANS. Equations 14, 19, and 20 were fit to the 6200 experimental data points with a $\Delta C_{p,\text{th}}$ of 5.40 kcal mol⁻¹ K⁻¹ and an x_0 of 310.15 K. The fitted curve and fluorescence trace are fully superposed within the experimental range of temperatures.

Information). For RPSA(2–295), we analyzed the unfolding profile with equations corresponding to a three-state system (eqs 14, 19, and 20). The following parameters were obtained: $T_{m1} = 307.40 \pm 0.14$ K, $\Delta H_{m1} = 75.45 \pm 0.78$ kcal mol⁻¹, $T_{m2} = 164.55 \pm 8.03$ K, $\Delta H_{m2} = -73.77 \pm 1.65$ kcal mol⁻¹, $\Delta C_{p1} = 4.13 \pm 0.07$ kcal mol⁻¹ K⁻¹, $\Delta C_{p2} = \Delta C_{p,\text{th}} - \Delta C_{p1} = 1.27 \pm 0.07$ kcal mol⁻¹ K⁻¹, and $n_i = 1.59 \pm 0.02$. The profile showed a

first highly cooperative transition around 34.1 °C ($f_n = 0.5$ at 307.23 K; $\Delta C_{p1} = 4.13 \text{ kcal mol}^{-1} \text{ K}^{-1}$), followed by a second weakly cooperative transition around 38.8 °C ($f_u = 0.5$ at 311.95 K; $\Delta C_{p2} = 1.27 \text{ kcal mol}^{-1} \text{ K}^{-1}$). The first transition led to an intermediate I whose molar fraction (f_i) was equal to 0.57 at 37 °C and whose molar fluorescence (Y_i) was 1.59-fold higher than Y_n of the native protein at the same temperature. Thus, we could directly observe an intermediate state of folding at 37 °C for full-length RPSA.

Interaction between the N- and C-Domains. The deconvolutions of the far-UV CD spectra showed that the secondary structure content for RPSA was not exactly the weighted sum of the secondary structure contents for its isolated N- and C-domains (Table 2). Therefore, we tested whether the isolated N- and C-domains could interact together by an indirect ELISA at 25 °C. These experiments showed a weak but specific interaction between RPSA(2–209) in the immobile phase and Flag-RPSA(225–295) in the liquid phase for concentrations of the latter higher than 1 μM (Figure 9).

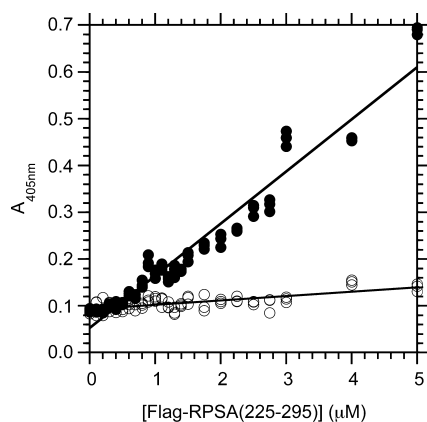


Figure 9. Interaction between Flag-RPSA(225–295) and RPSA(2–209), as assayed by an indirect ELISA at 25 °C. (●) RPSA(2–209) was immobilized at 2 $\mu\text{g/mL}$ in PBS; (○) PBS alone was used as a control. The captured Flag-RPSA(225–295) was detected with a conjugate between alkaline phosphatase and an antibody to the Flag tag. The slopes of the fitted lines are in a 12:1 ratio.

This interaction could be significant in full-length RPSA because the two domains are covalently linked in this context and therefore their effective (or apparent) concentrations are high.

DISCUSSION

Folding State of the Isolated C-Domain. A first objective of this study consisted of characterizing the folding state of the C-domain, for which no experimental structural data existed. We showed the following points at 20 °C for one of the two C-domains or the other, RPSA(210–295) and RPSA(225–295). (i) The far-UV CD spectra of the two C-domains were characteristic of proteins that comprise a majority of random coil residues. (ii) The λ_{max} values of the fluorescence spectra were equal to 351 nm for the two C-domains and therefore consistent with solvent-exposed Trp residues. (iii) The profile of unfolding for RPSA(210–295), induced with urea and monitored through its intrinsic fluorescence, was linear, noncooperative, and close to the profile of interaction between the free Trp amino acid and urea. Its profiles of unfolding by heat, monitored either by its intrinsic fluorescence or by far-UV

CD, were also noncooperative. Therefore, the denaturation of the C-domain involved a continuum of conformational states. (iv) The near-UV CD spectra indicated that some of the Phe and Trp residues of the two C-domains interacted with their electronic and structural environment. Remarkably, Phe and Trp residues are associated in two of the five repetitions of the C-domains: $^{225}\text{EEFQGEWTA}$ and $^{260}\text{QQFPTEDWSA}$. (v) RPSA(210–295) was not in a molten globule state because it had no regular secondary structure and did not bind ANS.⁶⁰

We concluded from these results that the isolated C-domain was in an intrinsically disordered state, with Trp residues exposed to the solvent and some groups of residues in local interactions. Our conclusions were consistent with computations that we made for full-length RPSA through MeDor, a metasever for predicting protein disorder.⁴⁷ Most programs included in MeDor predicted residues 210–295 of RPSA were in a disordered conformation (Figure S20 of the Supporting Information). We discuss below whether the folding states of the C-domain are identical when it is isolated or integrated in full-length RPSA.

Multiple Folding States of the N-Domain. A second objective of this study consisted of characterizing the unfolding equilibria and stability of the N-domain. We showed the following points. The unfolding equilibria of RPSA(2–209) and RPSA(2–220), induced with urea at 20 °C and monitored through their intrinsic fluorescence, were modeled with a three-state system, N, I, and U (Table 3 and Figure 4). Remarkably, the molar fraction of intermediate I was equal to 0.96 at a concentration of urea equal to 2.74 M for RPSA(2–209). Therefore, there were experimental conditions under which I was the only conformational state, in a quasi-pure form, and it should be possible to characterize this intermediate further. The global stability of RPSA(2–209) was equal to $11.5 \pm 2.5 \text{ kcal mol}^{-1}$. This value was consistent with the stabilities of other monomeric proteins that possess a folding intermediate.⁶¹

The unfolding equilibria of the two N-domains, induced with heat and monitored through their intrinsic fluorescence, were also modeled with a three-state system (Table 4 and Figure S12 of the Supporting Information). Native state N represented 33% of the N-domain molecules and intermediate state I 62% of them at 37 °C, i.e., the temperature of the human body. In contrast, state N represented 97% of the N-domain molecules at 17 °C, 96% at 20 °C, and 91% at 25 °C (Table 5). In unfolding with urea at 20 °C, the quasi-totality of the molecules were therefore in native state N in the absence of urea. The X-ray structure of the N-domain has been determined from crystals grown at 17 °C and therefore could represent a frozen state of the molecular structure. The global stability ($\Delta G = \Delta G_1 + \Delta G_2$) of RPSA(2–220) was maximal for a temperature of 17.9 °C, i.e., very close to that at which the crystals were obtained.

The unfolding equilibria of the N-domains, induced with urea or heat, were also monitored through the extrinsic fluorescence of ANS. These experiments confirmed that the N-domain unfolded through a three-state equilibrium, and they showed that the intermediate state I bound ANS. The thermodynamic parameters obtained when the unfolding equilibria were monitored either through the extrinsic fluorescence of ANS or through the intrinsic fluorescence of proteins cannot be compared directly because the equations that we used did not take into account the interactions between ANS and the proteins under study, for the sake of simplicity, even though ANS can influence the unfolding of proteins.⁶²

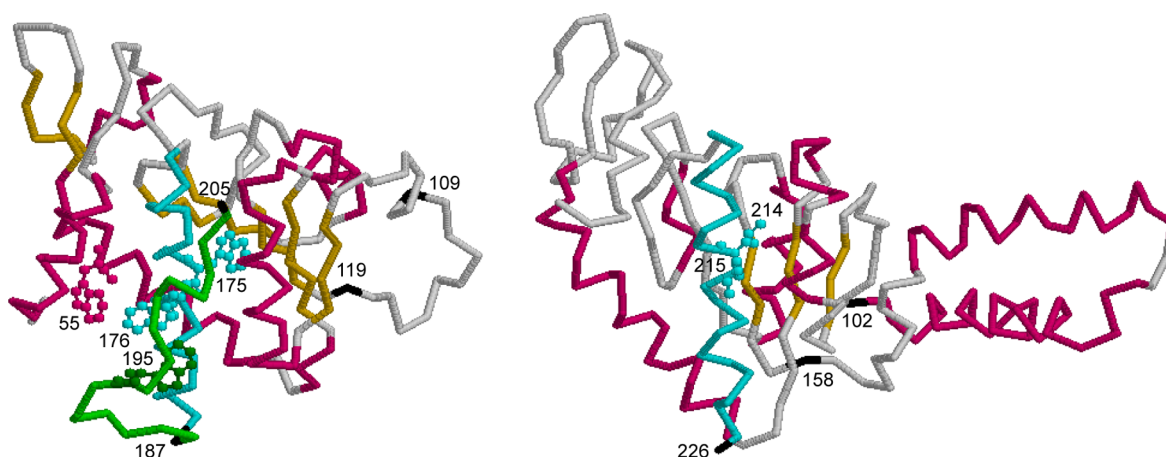


Figure 10. Comparison of the structures of the N-domain (residues 1–220) of human RPSA and *E. coli* RPS2. The RPSA structure on the left and the RPS2 structure on the right are represented by the chain of their C_{α} atoms. The two structures have been aligned through the α -helices (cyan) that carry the palindromic sequence 173 LMWWML of RPSA or the homologous sequence 212 LYLGAV of RPS2 (numbering from the initiator Met). The last visible residue in the structure of RPS2 is Ser226, which is homologous to Gly187 in RPSA. The Thr188–Arg205 segment of RPSA, which folds back on the palindromic sequence, is colored green. The other α -helices are colored magenta and the β -sheets yellow. The four Trp residues of the N-domain of RPSA, Trp55, Trp175, Trp176, and Trp195, and the two residues of RPS2, Leu214 and Gly215, are represented as balls and sticks. RPS2 includes a long hairpin between residues Thr102 and Pro158 that is absent between the homologous residues of RPSA, Thr109 and Pro119, respectively.

Together, the data summarized in this paragraph show that the N-domain existed in an intermediate state of folding that was highly populated under some conditions, in particular at 37 °C or in 2.75 M urea, and different from native state N whose structure has been determined at 17 °C.

Multiple Folding States of Full-Length RPSA. Full-length RPSA is the protein species that is present in vivo. Therefore, it was necessary to test whether the conclusions that we drew from the analysis of the isolated N- and C-domains were valid for the full-length protein. The unfolding profiles of RPSA(2–295), induced with urea or heat and monitored through its intrinsic fluorescence, showed a single transition. It is likely that the contributions of the four Trp residues of the N-domain to fluorescence were diluted by those of the six Trp residues of the C-domain, and that this dilution effect masked the two transitions. Consistent with this interpretation, the half-transition occurred at 2.69 M urea, i.e., approximately at the urea concentration (2.74 M) at which intermediate I of the N-domain had its maximal molar fraction (Table 3). We observed an intermediate state of RPSA(2–295) between 32 and 42 °C by analyzing its unfolding equilibria, induced with heat and monitored through the protein intrinsic fluorescence, with a phase diagram (Figure 6). We also observed an intermediate by monitoring the unfolding equilibria through the extrinsic fluorescence of ANS, both with urea and with heat as denaturing agents. At 37 °C, the molar fraction of intermediate I was equal to 0.57, i.e., half the molecules of RPSA(2–295) (Figure 8 and Results). Therefore, the intermediate could exist in vivo under physiological conditions. RPSA could be in equilibrium between the N and I states at 37 °C in vivo, which would give it some structural plasticity and allow it to conduct its different functions.

Identity of the Intermediate States. We observed intermediate states of folding, which we named I in a generic way, for different derivatives of RPSA, namely, RPSA(2–209), RPSA(2–220), and RPSA(2–295), and under different experimental conditions. Were they structurally identical? We monitored the equilibria of unfolding, induced with urea,

through the intensity of fluorescence of either aromatic residues or ANS. The concentrations of urea at which the molar fraction of intermediate I was maximal were very close in the two types of experiments and for the three tested proteins: $f_i^{-1}(\max f_i) = 2.74$ M versus 2.82 M for RPSA(2–209), 2.97 M versus 2.78 M for RPSA(2–220), and 2.84 M for RPSA(2–295) [Tables 3 and 6; for RPSA(2–295), we quantified the molar fraction of I only in the experiment with ANS]. These values suggested the following conclusions with regard to the intermediates obtained with urea. (i) The same intermediate of the N-domain was detected through the two fluorescent probes, aromatic residues and ANS. (ii) The intermediates of the N-domain and full-length RPSA had conformations that corresponded to each other. (iii) The intermediate displayed binding sites for ANS that did not exist in the native state.

In the experiments with heat, the first transition in the profiles of unfolding equilibria occurred at the same temperature for RPSA(2–295) when ANS was used as a fluorescent probe ($f_n = 0.5$ at 307.23 K) and for RPSA(2–209) and RPSA(2–220) when the aromatic residues were used ($f_n = 0.5$ at 307.87 and 307.67 K). These values suggested again that the intermediates of the N-domain and full-length protein had conformations that corresponded to each other.

To compare the conformational states of RPSA(2–209) between unfolding with urea and heat, we used their molar intensities of intrinsic fluorescence (Y_n , Y_i , and Y_u) at 20 °C in the absence of urea. The ratio Y_i/Y_n was equal to 0.67 in the experiments with urea and 0.59 in the experiments with heat. Y_u/Y_n was equal to 0.32 in the experiments with urea and 0.29 in the experiments with heat (Tables 3 and 5). Thus, the relative molar intensities of states I and U of RPSA(2–209) had similar values at 20 °C in the two types of unfolding experiments, with urea or heat.

RPSA(2–209) lost ~50% of its molar fluorescence intensity during the transition from N to I, induced with urea, because $(Y_n - Y_i)/(Y_n - Y_u) = (1 - n_i)/(1 - n_u)$, and 50% during the transition from I to U (Table 3). Therefore, it is tempting to speculate that two of the four Trp residues of RPSA(2–209)

became exposed to the solvent during the transition from N to I. An analysis of the structure of the N-domain showed that the four Trp residues are buried within the protein (Figure 10). Residue Trp175 is fully buried in the protein core. Trp176 makes many contacts with 5 of the 11 C-terminal residues (195–205) of the N-domain, i.e., Trp195, Val197, Met198, Pro199, and Tyr102, whereas Trp175 does not make any contact with this segment. The interaction between residues 195–205 and the remainder of the N-domain might be abolished in intermediate I, and thus, Trp176 and Trp195 might become exposed to the solvent. This hypothesis is consistent with the results of a molecular dynamics simulation of the N-domain of RPSA at 300 K (27 °C). The simulation shows that the loop of residues 188–197 is highly flexible and undergoes a conformational switch that partially exposes residue Arg180 (see below).⁶³

In summary, our results and the available data suggest that we observed a single intermediate in our various experiments and that it could correspond to the disassembly of residues 195–205.

Isolated and Integrated Domains. The isolated N-domain folds in a manner that is independent of the C-domain,⁵ whereas the isolated C-domain is mainly in a disordered state. However, we showed the existence of a weak but specific interaction between the positively charged RPSA(2–209) domain and the negatively charged Flag-RPSA(225–295) domain by indirect ELISAs (Figure 9). This interaction could be significant in the context of full-length RPSA. We also showed by far-UV CD experiments that the content of α -helical residues was significantly higher for RPSA(2–295) than for the union of the isolated RPSA(2–209) and RPSA(210–295) domains and the content of random coil residues significantly lower (Table 2). The N- and C-domains might interact together, and the C-domain might have a conformation more ordered when it is integrated into the full-length protein than when it is isolated.

Laminin Binding. It has been proposed that the segment of RPSA that comprises residues 161–180 and is named peptide G belongs to the binding sites of laminin^{36,64} and prion.^{55,65} Antibodies to a synthetic peptide that corresponds to residues 165–184 of RPSA specifically recognize human RPSA, purified from liver metastases of breast carcinomas or present on the surface of living nonpermeabilized tumor cells.⁶⁶ These segments contain the palindromic sequence ¹⁷³LMWWML¹⁷⁸, which is conserved in all metazoans.³ In the structure of RPSA(2–220), the only residues of peptide G that have a solvent accessible surface area (ASA) higher than 10% or 10 Å² are Asn164 (9.7%, 16.2 Å²), Lys166 (75%, 147.0 Å²), Ala168 (26.1%, 20.7 Å²), His169 (50.6%, 100.6 Å²), and Arg180 (4.2%, 10.7 Å²). A change of Lys166 into Ala does not affect the binding of laminin in an ELISA at 37 °C.⁶⁷ However, if one assumes that the segment of residues 195–205 disassembles at 37 °C, then the ASA increases for several residues of peptide G: Leu173 (12.7%, 23 Å²), Trp176 (46.6%, 121.1 Å²), and Ala179 (9.2%, 10.5 Å²). The major change involves Trp176, whose side chain would become highly accessible (Figure 10). Thus, one cannot exclude the possibility that peptide G participates in the binding of some ligands at 37 °C. Moreover, the binding of a ligand could shift the equilibrium between the N and I states toward the I state below 37 °C.

RPSA and the Structure of the Ribosome. In the X-ray structure of the *E. coli* ribosome, residues 1–8 and 227–241 of RPS2, the homologue of the N-domain of RPSA, are not visible

in the electron density map (numbering from the initial Met).⁶⁸ Leu214 and Gly215 of *E. coli* RPS2 are equivalent to Trp175 and Trp176 of RPSA, and Ser226 of RPS2 is equivalent to Gly187 of RPSA. Therefore, the α -helix of RPS2 that includes Leu214 and Gly215 is directly accessible to the solvent and not buried by interaction with a C-terminal segment as in the crystal structure of RPSA (Figure 10).

The sequences of the RPS2 proteins from *E. coli* and *T. thermophilus* include a long segment, between residues Thr102 and Pro158, which is absent from the sequences of *A. fulgidus* RPS2 and *H. sapiens* RPSA (Figure S21 of the Supporting Information). In the X-ray structures of the *E. coli* and *T. thermophilus* ribosomes, these segments form a long ordered hairpin that points outside of the protein and interacts with the 16S RNA.^{68,69} The C-domain of RPSA, which is absent from the prokaryotic RPS2, is essential for the binding of RPSA to the ribosome, and it interacts with 18S RNA through residues 236–262.⁷ Therefore, the C-domain of RPSA might order and partially fold upon its interaction with the 18S RNA and be a functional equivalent of residues 103–157 in prokaryotic RPS2.

Perspectives. We have reported the bacterial production of RPSA and its domains in quantities and purities that are adequate for in vitro biophysical, structural, and functional studies. In particular, it should be possible to characterize more thoroughly the intermediate folding state of the N-domain, to assay and quantify the interactions between the various RPSA derivatives and their ligands in vitro, to map the corresponding binding sites, and, more generally, to study in detail the relations among the structure, folding, and function of RPSA. The results of such studies will serve applications against cancer and the various pathogens that interact with RPSA. We have undertaken such studies, and it is worth mentioning here that the isolated N- and C-domains have both idiosyncratic and shared functions (manuscript in preparation). Thus, RPSA belongs to the large family of human proteins that have intrinsically disordered regions, and it appears to be an example of proteins whose structure, determined in their free state from crystals grown at low temperatures, might not fully explain their behavior at the body temperature and in the presence of ligands.

■ ASSOCIATED CONTENT

📄 Supporting Information

Analysis of the RPSA derivatives by SDS–PAGE under reducing conditions (Figure S1), preparative gel filtration of RPSA(210–295) (Figure S2), comparison of the near-UV CD spectra of RPSA(210–295) and RPSA(225–295) (Figure S3), fluorescence spectra of RPSA(210–295), RPSA(2–209), RPSA(2–220), and RPSA(2–295) at 20 °C in buffer D in the presence or absence of 8 M urea (Figures S4–S7), unfolding equilibria of RPSA(2–220), RPSA(210–295), and RPSA(2–295) induced with urea at 20 °C in buffer D and monitored through their intrinsic fluorescence (Figures S8–S10), unfolding equilibria of RPSA(2–220), RPSA(210–295), and RPSA(2–295) induced with heat in buffer D and monitored through their intrinsic fluorescence (Figures S11, S13, and S15), unfolding equilibria of RPSA(210–295) induced with heat in buffer C and monitored through its CD signal at 207 nm (Figure S14), molar fractions f_n , f_i , and f_u of the native N, intermediate I, and unfolded U states, respectively, of RPSA(2–209) in buffer D as a function of temperature (Figure S12), phase diagram for the unfolding of RPSA(2–209) induced with heat in buffer D and monitored

through its intrinsic fluorescence (Figure S16), unfolding equilibria of RPSA(2–209) induced with urea at 20 °C in buffer E and monitored through the fluorescence intensity *Y* of ANS (Figure S17), unfolding equilibria of RPSA(2–209) and RPSA(2–220) induced with heat in buffer F and monitored through the fluorescence intensity *Y* of ANS (Figures S18 and S19), predictions of order and disorder in human RPSA as obtained with the metasever MeDor (Figure S20), and multiple-sequence alignment for the human RPSA protein and three prokaryotic RPS2 proteins (Figure S21). This material is available free of charge via the Internet at <http://pubs.acs.org>.

AUTHOR INFORMATION

Corresponding Author

*Institut Pasteur, CNRS URA3012, and Unit of Molecular Prevention and Therapy of Human Diseases, 28 rue Docteur Roux, 75724 Paris Cedex 15, France. Telephone: +33-1-45688379. Fax: +33-1-40613533. E-mail: hugues.bedouelle@pasteur.fr.

Funding

This work was supported by a Pasteur-Weizmann short-term grant (M.B.O.-A.).

Notes

The authors declare no competing financial interest.

ACKNOWLEDGMENTS

We thank Patrick England for access to the Plate-forme de Biophysique des Macromolécules et de leurs Interactions; Joseph J. B. Cockburn and Pascal Lenormand for performing the gel filtration and mass spectrometry analyses, respectively; P. England and Alexandre Chenal for advice; Nicole Guiso for her constant interest; one reviewer for suggesting that we publish our Supporting Information and bringing the MeDor metasever to our attention; and another reviewer for bringing the method of the phase diagrams to our attention.

REFERENCES

- (1) Rao, C. N., Castronovo, V., Schmitt, M. C., Wewer, U. M., Claysmith, A. P., Liotta, L. A., and Sobel, M. E. (1989) Evidence for a precursor of the high-affinity metastasis-associated murine laminin receptor. *Biochemistry* 28, 7476–7486.
- (2) Jackers, P., Minoletti, F., Belotti, D., Clausse, N., Sozzi, G., Sobel, M. E., and Castronovo, V. (1996) Isolation from a multigene family of the active human gene of the metastasis-associated multifunctional protein 37LRP/p40 at chromosome 3p21.3. *Oncogene* 13, 495–503.
- (3) Ardini, E., Pesole, G., Tagliabue, E., Magnifico, A., Castronovo, V., Sobel, M. E., Colnaghi, M. I., and Menard, S. (1998) The 67-kDa laminin receptor originated from a ribosomal protein that acquired a dual function during evolution. *Mol. Biol. Evol.* 15, 1017–1025.
- (4) Nelson, J., McFerran, N. V., Pivato, G., Chambers, E., Doherty, C., Steele, D., and Timson, D. J. (2008) The 67 kDa laminin receptor: Structure, function and role in disease. *Biosci. Rep.* 28, 33–48.
- (5) Jamieson, K. V., Wu, J., Hubbard, S. R., and Meruelo, D. (2008) Crystal structure of the human laminin receptor precursor. *J. Biol. Chem.* 283, 3002–3005.
- (6) Malygin, A. A., Bondarenko, E. I., Ivanisenko, V. A., Protopopova, E. V., Karpova, G. G., and Loktev, V. B. (2009) C-terminal fragment of human laminin-binding protein contains a receptor domain for venezuelan equine encephalitis and tick-borne encephalitis viruses. *Biochemistry (Moscow, Russ. Fed.)* 74, 1328–1336.
- (7) Malygin, A. A., Babaylova, E. S., Loktev, V. B., and Karpova, G. G. (2011) A region in the C-terminal domain of ribosomal protein SA required for binding of SA to the human 40S ribosomal subunit. *Biochimie* 93, 612–617.
- (8) Liotta, L. A., Horan Hand, P., Rao, C. N., Bryant, G., Barsky, S. H., and Schlom, J. (1985) Monoclonal antibodies to the human laminin receptor recognize structurally distinct sites. *Exp. Cell Res.* 156, 117–126.
- (9) Castronovo, V., Claysmith, A. P., Barker, K. T., Cioce, V., Krutzsch, H. C., and Sobel, M. E. (1991) Biosynthesis of the 67 kDa high affinity laminin receptor. *Biochem. Biophys. Res. Commun.* 177, 177–183.
- (10) Landowski, T. H., Dratz, E. A., and Starkey, J. R. (1995) Studies of the structure of the metastasis-associated 67 kDa laminin binding protein: Fatty acid acylation and evidence supporting dimerization of the 32 kDa gene product to form the mature protein. *Biochemistry* 34, 11276–11287.
- (11) Buto, S., Tagliabue, E., Ardini, E., Magnifico, A., Ghirelli, C., van den Brule, F., Castronovo, V., Colnaghi, M. I., Sobel, M. E., and Menard, S. (1998) Formation of the 67-kDa laminin receptor by acylation of the precursor. *J. Cell. Biochem.* 69, 244–251.
- (12) Rush, J., Moritz, A., Lee, K. A., Guo, A., Goss, V. L., Spek, E. J., Zhang, H., Zha, X. M., Polakiewicz, R. D., and Comb, M. J. (2005) Immunoaffinity profiling of tyrosine phosphorylation in cancer cells. *Nat. Biotechnol.* 23, 94–101.
- (13) Rao, N. C., Barsky, S. H., Terranova, V. P., and Liotta, L. A. (1983) Isolation of a tumor cell laminin receptor. *Biochem. Biophys. Res. Commun.* 111, 804–808.
- (14) Lesot, H., Kuhl, U., and Mark, K. V. (1983) Isolation of a laminin-binding protein from muscle cell membranes. *EMBO J.* 2, 861–865.
- (15) Starkey, J. R., Uthayakumar, S., and Berglund, D. L. (1999) Cell surface and substrate distribution of the 67-kDa laminin-binding protein determined by using a ligand photoaffinity probe. *Cytometry* 35, 37–47.
- (16) Gauczynski, S., Peyrin, J. M., Haik, S., Leucht, C., Hundt, C., Rieger, R., Krasemann, S., Deslys, J. P., Dormont, D., Lasmezas, C. I., and Weiss, S. (2001) The 37-kDa/67-kDa laminin receptor acts as the cell-surface receptor for the cellular prion protein. *EMBO J.* 20, 5863–5875.
- (17) Auth, D., and Brawerman, G. (1992) A 33-kDa polypeptide with homology to the laminin receptor: Component of translation machinery. *Proc. Natl. Acad. Sci. U.S.A.* 89, 4368–4372.
- (18) Tohgo, A., Takasawa, S., Munakata, H., Yonekura, H., Hayashi, N., and Okamoto, H. (1994) Structural determination and characterization of a 40 kDa protein isolated from rat 40 S ribosomal subunit. *FEBS Lett.* 340, 133–138.
- (19) Vladimirov, S. N., Ivanov, A. V., Karpova, G. G., Musolyamov, A. K., Egorov, T. A., Thiede, B., Wittmann-Liebold, B., and Otto, A. (1996) Characterization of the human small-ribosomal-subunit proteins by N-terminal and internal sequencing, and mass spectrometry. *Eur. J. Biochem.* 239, 144–149.
- (20) Sato, M., Saeki, Y., Tanaka, K., and Kaneda, Y. (1999) Ribosome-associated protein LBP/p40 binds to S21 protein of 40S ribosome: analysis using a yeast two-hybrid system. *Biochem. Biophys. Res. Commun.* 256, 385–390.
- (21) Kinoshita, K., Kaneda, Y., Sato, M., Saeki, Y., Wataya-Kaneda, M., and Hoffmann, A. (1998) LBP-p40 binds DNA tightly through associations with histones H2A, H2B, and H4. *Biochem. Biophys. Res. Commun.* 253, 277–282.
- (22) Salama, R. H., Muramatsu, H., Zou, K., Inui, T., Kimura, T., and Muramatsu, T. (2001) Midkine binds to 37-kDa laminin binding protein precursor, leading to nuclear transport of the complex. *Exp. Cell Res.* 270, 13–20.
- (23) O'Donohue, M. F., Choessel, V., Faubladiet, M., Fichant, G., and Gleizes, P. E. (2010) Functional dichotomy of ribosomal proteins during the synthesis of mammalian 40S ribosomal subunits. *J. Cell Biol.* 190, 853–866.
- (24) Terranova, V. P., Rao, C. N., Kalebic, T., Margulies, I. M., and Liotta, L. A. (1983) Laminin receptor on human breast carcinoma cells. *Proc. Natl. Acad. Sci. U.S.A.* 80, 444–448.

- (25) Fatehullah, A., Doherty, C., Pivato, G., Allen, G., Devine, L., Nelson, J., and Timson, D. J. (2010) Interactions of the 67 kDa laminin receptor and its precursor with laminin. *Biosci. Rep.* 30, 73–79.
- (26) Berno, V., Porrini, D., Castiglioni, F., Campiglio, M., Casalini, P., Pupa, S. M., Balsari, A., Menard, S., and Tagliabue, E. (2005) The 67 kDa laminin receptor increases tumor aggressiveness by remodeling laminin-1. *Endocr.-Relat. Cancer* 12, 393–406.
- (27) Wang, K. S., Kuhn, R. J., Strauss, E. G., Ou, S., and Strauss, J. H. (1992) High-affinity laminin receptor is a receptor for Sindbis virus in mammalian cells. *J. Virol.* 66, 4992–5001.
- (28) Thepparit, C., and Smith, D. R. (2004) Serotype-specific entry of dengue virus into liver cells: Identification of the 37-kilodalton/67-kilodalton high-affinity laminin receptor as a dengue virus serotype 1 receptor. *J. Virol.* 78, 12647–12656.
- (29) Tio, P. H., Jong, W. W., and Cardoso, M. J. (2005) Two dimensional VOPBA reveals laminin receptor (LAMR1) interaction with dengue virus serotypes 1, 2 and 3. *J. Virol.* 79, 25.
- (30) Akache, B., Grimm, D., Pandey, K., Yant, S. R., Xu, H., and Kay, M. A. (2006) The 37/67-kilodalton laminin receptor is a receptor for adeno-associated virus serotypes 8, 2, 3, and 9. *J. Virol.* 80, 9831–9836.
- (31) Kim, K. J., Chung, J. W., and Kim, K. S. (2005) 67-kDa laminin receptor promotes internalization of cytotoxic necrotizing factor 1-expressing *Escherichia coli* K1 into human brain microvascular endothelial cells. *J. Biol. Chem.* 280, 1360–1368.
- (32) Orihuela, C. J., Mahdavi, J., Thornton, J., Mann, B., Wooldridge, K. G., Abouseada, N., Oldfield, N. J., Self, T., Ala'Aldeen, D. A., and Tuomanen, E. I. (2009) Laminin receptor initiates bacterial contact with the blood brain barrier in experimental meningitis models. *J. Clin. Invest.* 119, 1638–1646.
- (33) Kim, K., Li, L., Kozlowski, K., Suh, H. S., Cao, W., and Ballermann, B. J. (2005) The protein phosphatase-1 targeting subunit TIMAP regulates LAMR1 phosphorylation. *Biochem. Biophys. Res. Commun.* 338, 1327–1334.
- (34) Umeda, D., Yano, S., Yamada, K., and Tachibana, H. (2008) Green tea polyphenol epigallocatechin-3-gallate signaling pathway through 67-kDa laminin receptor. *J. Biol. Chem.* 283, 3050–3058.
- (35) Scheiman, J., Jamieson, K. V., Ziello, J., Tseng, J. C., and Meruelo, D. (2010) Extraribosomal functions associated with the C terminus of the 37/67 kDa laminin receptor are required for maintaining cell viability. *Cell Death Dis.* 1, e42.
- (36) Kazmin, D. A., Hoyt, T. R., Taubner, L., Teintze, M., and Starkey, J. R. (2000) Phage display mapping for peptide 11 sensitive sequences binding to laminin-1. *J. Mol. Biol.* 298, 431–445.
- (37) Radivojac, P., Iakoucheva, L. M., Oldfield, C. J., Obradovic, Z., Uversky, V. N., and Dunker, A. K. (2007) Intrinsic disorder and functional proteomics. *Biophys. J.* 92, 1439–1456.
- (38) Wright, P. E., and Dyson, H. J. (2009) Linking folding and binding. *Curr. Opin. Struct. Biol.* 19, 31–38.
- (39) Uversky, V. N., and Dunker, A. K. (2010) Understanding protein non-folding. *Biochim. Biophys. Acta* 1804, 1231–1264.
- (40) Santoro, M. M., and Bolen, D. W. (1988) Unfolding free energy changes determined by the linear extrapolation method. 1. Unfolding of phenylmethanesulfonyl α -chymotrypsin using different denaturants. *Biochemistry* 27, 8063–8068.
- (41) Pace, C. N. (1986) Determination and analysis of urea and guanidine hydrochloride denaturation curves. *Methods Enzymol.* 131, 266–280.
- (42) Myers, J. K., Pace, C. N., and Scholtz, J. M. (1995) Denaturant m values and heat capacity changes: Relation to changes in accessible surface areas of protein unfolding. *Protein Sci.* 4, 2138–2148.
- (43) Monsellier, E., and Bedouelle, H. (2005) Quantitative measurement of protein stability from unfolding equilibria monitored with the fluorescence maximum wavelength. *Protein Eng. Des. Sel.* 18, 445–456.
- (44) Arnau, J., Lauritzen, C., Petersen, G. E., and Pedersen, J. (2006) Current strategies for the use of affinity tags and tag removal for the purification of recombinant proteins. *Protein Expression Purif.* 48, 1–13.
- (45) Renard, M., Belkadi, L., Hugo, N., England, P., Altschuh, D., and Bedouelle, H. (2002) Knowledge-based design of reagentless fluorescent biosensors from recombinant antibodies. *J. Mol. Biol.* 318, 429–442.
- (46) Larkin, M. A., Blackshields, G., Brown, N. P., Chenna, R., McGettigan, P. A., McWilliam, H., Valentin, F., Wallace, I. M., Wilm, A., Lopez, R., Thompson, J. D., Gibson, T. J., and Higgins, D. G. (2007) Clustal W and Clustal X version 2.0. *Bioinformatics* 23, 2947–2948.
- (47) Lieutaud, P., Canard, B., and Longhi, S. (2008) MeDor: A metasever for predicting protein disorder. *BMC Genomics* 9 (Suppl. 2), S25.
- (48) Rice, P., Longden, I., and Bleasby, A. (2000) EMBOSS: The European Molecular Biology Open Software Suite. *Trends Genet.* 16, 276–277.
- (49) Compton, L. A., and Johnson, W. C., Jr. (1986) Analysis of protein circular dichroism spectra for secondary structure using a simple matrix multiplication. *Anal. Biochem.* 155, 155–167.
- (50) Whitmore, L., and Wallace, B. A. (2004) DICROWEB, an online server for protein secondary structure analyses from circular dichroism spectroscopic data. *Nucleic Acids Res.* 32, W668–W673.
- (51) Vriend, G. (1990) WHAT IF: A molecular modeling and drug design program. *J. Mol. Graphics* 8, 52–56.
- (52) Kaessmann, H., Zollner, S., Nekrutenko, A., and Li, W. H. (2002) Signatures of domain shuffling in the human genome. *Genome Res.* 12, 1642–1650.
- (53) Fedorov, A., Roy, S., Cao, X., and Gilbert, W. (2003) Phylogenetically older introns strongly correlate with module boundaries in ancient proteins. *Genome Res.* 13, 1155–1157.
- (54) Graceffa, P., Jancso, A., and Mabuchi, K. (1992) Modification of acidic residues normalizes sodium dodecyl sulfate-polyacrylamide gel electrophoresis of caldesmon and other proteins that migrate anomalously. *Arch. Biochem. Biophys.* 297, 46–51.
- (55) Hundt, C., Peyrin, J. M., Haik, S., Gauczynski, S., Leucht, C., Rieger, R., Riley, M. L., Deslys, J. P., Dormont, D., Lasmezas, C. I., and Weiss, S. (2001) Identification of interaction domains of the prion protein with its 37-kDa/67-kDa laminin receptor. *EMBO J.* 20, 5876–5886.
- (56) Woody, R. W. (1994) Contributions of tryptophan side chains to the far-ultraviolet circular dichroism of proteins. *Eur. Biophys. J.* 23, 253–262.
- (57) Pain, R. (2005) Determining the CD spectrum of a protein, *Current Protocols in Protein Science*, Chapter 7, Unit 7.6, Wiley, New York.
- (58) Kuznetsova, I. M., Turoverov, K. K., and Uversky, V. N. (2004) Use of the phase diagram method to analyze the protein unfolding-refolding reactions: Fishing out the “invisible” intermediates. *J. Proteome Res.* 3, 485–494.
- (59) Stryer, L. (1965) The interaction of a naphthalene dye with apomyoglobin and apohemoglobin. A fluorescent probe of non-polar binding sites. *J. Mol. Biol.* 13, 482–495.
- (60) Semisotnov, G. V., Rodionova, N. A., Razgulyaev, O. I., Uversky, V. N., Gripas, A. F., and Gilmanshin, R. I. (1991) Study of the “molten globule” intermediate state in protein folding by a hydrophobic fluorescent probe. *Biopolymers* 31, 119–128.
- (61) Kumar, M. D., Bava, K. A., Gromiha, M. M., Prabakaran, P., Kitajima, K., Uedaira, H., and Sarai, A. (2006) ProTherm and ProNIT: Thermodynamic databases for proteins and protein-nucleic acid interactions. *Nucleic Acids Res.* 34, D204–D206.
- (62) Matulis, D., Baumann, C. G., Bloomfield, V. A., and Lovrien, R. E. (1999) 1-Anilino-8-naphthalene sulfonate as a protein conformational tightening agent. *Biopolymers* 49, 451–458.
- (63) Di Giovanni, C., Grottesi, A., and Lavecchia, A. (2012) Conformational switch of a flexible loop in human laminin receptor determines laminin-1 interaction. *Eur. Biophys. J.* 41, 353–358.
- (64) Castronovo, V., Tarabozetti, G., and Sobel, M. E. (1991) Functional domains of the 67-kDa laminin receptor precursor. *J. Biol. Chem.* 266, 20440–20446.

- (65) Rieger, R., Edenhofer, F., Lasmezas, C. I., and Weiss, S. (1997) The human 37-kDa laminin receptor precursor interacts with the prion protein in eukaryotic cells. *Nat. Med.* 3, 1383–1388.
- (66) Wewer, U. M., Tarabozetti, G., Sobel, M. E., Albrechtsen, R., and Liotta, L. A. (1987) Role of laminin receptor in tumor cell migration. *Cancer Res.* 47, 5691–5698.
- (67) Jamieson, K. V., Hubbard, S. R., and Meruelo, D. (2011) Structure-guided identification of a laminin binding site on the laminin receptor precursor. *J. Mol. Biol.* 405, 24–32.
- (68) Schuwirth, B. S., Borovinskaya, M. A., Hau, C. W., Zhang, W., Vila-Sanjurjo, A., Holton, J. M., and Cate, J. H. (2005) Structures of the bacterial ribosome at 3.5 Å resolution. *Science* 310, 827–834.
- (69) Wimberly, B. T., Brodersen, D. E., Clemons, W. M., Jr., Morgan-Warren, R. J., Carter, A. P., Vornrhein, C., Hartsch, T., and Ramakrishnan, V. (2000) Structure of the 30S ribosomal subunit. *Nature* 407, 327–339.